

Control of a Uniformly Magnetized Plasma with External Electric Fields

Peiyi Chen^{1*}, Rogerio Jorge^{2†}, Qin Li^{1†}, Yukun Yue^{1†}

^{1*}Department of Mathematics, University of Wisconsin-Madison, 480 Lincoln Drive, Madison, 53706, WI, USA.

²Department of Physics, University of Wisconsin-Madison, 1150 University Avenue, Madison, 53706, WI, USA.

*Corresponding author(s). E-mail(s): pchen345@wisc.edu;
Contributing authors: rogerio.jorge@wisc.edu; qinli@math.wisc.edu;
yyue24@math.wisc.edu;

†These authors contributed equally to this work.

Abstract

Stabilizing plasma dynamics through externally applied electric and magnetic fields is a fundamental control problem. We study this question for a plasma evolving under a uniform external magnetic field. Although the governing dynamics are nonlinear, a linear analysis based on the Laplace–Fourier transform yields actionable insight. In particular, by controlling the location of the roots of the dispersion relation, we propose a general control strategy that restores stability, with the free-streaming solution recovered as a special case. Numerical experiments for Gaussian equilibria and for the Dory–Guest–Harris instability show that the proposed control suppresses the unstable modes and stabilizes the dynamics, in agreement with our theoretical predictions.

Keywords: Plasma, Vlasov-Poisson equation, Control, Bernstein modes, Dory-Guest-Harris instability, External electric field, Uniform external magnetic field

1 Introduction

Plasma is often referred to as the fourth state of matter: an ionized gas consisting of free electrons and ions. It is ubiquitous in nature and plays a central role in astrophysical phenomena, and it also underlies the promise of controlled nuclear fusion. However,

plasma dynamics can be highly unstable. Near certain equilibria, even small perturbations may trigger rapid growth of instabilities and drive the system into strongly nonlinear, possibly turbulent, regimes, posing major challenges for both experiments and applications [1–3]. In fusion devices, for instance, one aims to maintain the plasma close to a stable equilibrium for as long as possible so that the energy remains primarily in kinetic form. Instabilities can instead induce a fast transfer of energy into electric fields and other channels, making energy extraction difficult. Motivated by these considerations, we study plasma control strategies aimed at stabilizing the dynamics near equilibrium.

In most experimental configurations, such as tokamaks [4], stellarators, and mirror machines, plasma is confined by an externally applied magnetic field. We focus on a regime in which the magnetic field lines are approximately straight, a setting exemplified by the LAPD (LArge Plasma Device) at UCLA [5]. In this case, the plasma dynamics can be modeled by the Vlasov–Poisson (VP) system under a uniform external magnetic field. Denoting the electron distribution $F(t, \mathbf{x}, \mathbf{v})$, the self-generated electric potential $V(t, \mathbf{x})$ and the associated self-generated electric field $\mathbf{E}(t, \mathbf{x})$, VP system writes:

$$\begin{aligned} \frac{dF}{dt} &= \frac{\partial F}{\partial t} + \mathbf{v} \cdot \nabla_{\mathbf{x}} F + (\mathbf{E} + \mathbf{v} \times \mathbf{B}) \cdot \nabla_{\mathbf{v}} F = 0, \\ \nabla_{\mathbf{x}}^2 V &= 1 - \int_{\mathbb{R}^3} F d\mathbf{v}, \\ \mathbf{E} &= -\nabla_{\mathbf{x}} V. \end{aligned} \tag{1.1}$$

where $\frac{dF}{dt}$ denotes the total time variation of F , $\mathbf{x} = (x_1, x_2, x_3)^\top \in \mathbb{T}^3$, $\mathbf{v} = (v_1, v_2, v_3)^\top \in \mathbb{R}^3$ are the spatial and velocity coordinates. $\mathbf{B} = (0, 0, B_0)^\top$ is the fixed external magnetic field pointing in the x_3 -direction, with $B_0 > 0$. For notational convenience, throughout the paper, we denote $\mathbf{x}_\perp := (x_1, x_2)^\top$, $\mathbf{v}_\perp := (v_1, v_2)^\top$.

The added external magnetic field brings features to the VP system compared to the one without them [6–11]. The foremost discovery is that the structure of equilibrium distributions has changed. Due to the impact of the external magnetic field, only distribution that has radial symmetry in $\mathbf{v}_\perp = (v_1, v_2)$ space can serve as equilibrium states. Throughout the paper, we write our equilibrium state as a separable function $\mu(\mathbf{v}) = \mu_\perp(\mathbf{v}_\perp)\mu_\parallel(v_3)$. As in the classical VP stability analysis, some equilibrium states are stable while others are not, depending on the profile of μ_\perp and μ_\parallel . In this paper, we place focus on two kinds of equilibrium states with μ_\perp being either a Gaussian or ring-shaped. The former was shown in [12] to have non-damping components of electric energy, and the latter can form Dory-Guest-Harris instability [13–15]. Another characteristic feature of the Vlasov–Poisson system in the presence of a uniform magnetic field is the appearance of Bernstein modes [12, 16, 17]. When \mathbf{B} is directed along the x_3 -axis, it is natural to distinguish the dynamics parallel and perpendicular to the field. Bernstein modes correspond to electrostatic waves with perpendicular wavevector, i.e. $k_\parallel = 0$; in our notation this means $\mathbf{k} = (k_1, k_2, 0)^\top$. This restriction places the focus on stability properties in the transverse plane $\mathbf{x}_\perp =$

(x_1, x_2) , where magnetization induces behavior distinct from the unmagnetized case. As a consequence, we confine ourselves to these modes in numerical simulations.

In fusion applications, it is of particular interest to control the stability of plasma, which includes enhancing the solution's stability in the stable regime and suppressing instability in the unstable regime. There are many possible approaches to achieve the task, and one strategy is to impose an external electric field. This amounts to adding an extra electric field $H = -\nabla\Phi$ to (1.1). Upon obtaining the stability analysis for different modes, we then investigate the design principle for developing such external electric fields with the goal of controlling the stability of (1.1).

To understand plasma dynamics, modes with $k_3 = 0$ are routinely investigated in order to assess the relative importance of drift-waves, the Kelvin-Helmholtz (KH) instability, and sheath physics in driving turbulence and setting its saturation levels [5]. Experimentally [18, 19], plasma transport in LAPD due to KH modes with $k_3 = 0$ is studied using an external biasing of the plasma relative to the chamber wall. Additionally, in the Mirabelle experiment [20], strong KH mode activity is obtained for various source profiles. Theoretically, the approximation $k_3 \ll k_1, k_2$ is typically employed in magnetized plasma systems due to the fact that the strong guide field leads to a separation of scales, with turbulence in x_1 and x_2 occurring on the gyro-radius scale and structures along x_3 being on the order of the macroscopic length L . These are the approximations used to model magnetized plasmas using either a fluid framework (e.g., MHD and drift-reduced Braginskii equations) or a kinetic one (e.g., drift-kinetic and gyrokinetic equations). Finally, besides KH and sheath modes, we mention the Gradient-driven Drift Coupling (GDC) instability, which, as an essentially $k_3 \simeq 0$ mode, is regarded as a candidate mechanism for turbulence in basic, space, and astrophysical plasmas [21].

A cornerstone to understand plasma dynamics is to derive and analyze the dispersion relation. This is closely tied to the PDE theory on the study of the operators' spectrum. In the context of VP system, a celebrated work on Landau damping was rigorously proved in [22]. The dispersion relation for the system with an external magnetic field was studied in [12], where the authors investigated the stability of the Bernstein modes for μ_{\parallel} being a Gaussian. Extending from their work, we removed the Gaussian assumption on μ and achieved a more general dispersion relation.

The plasma control problem has also been extensively studied in the literature. It is particularly prominent in the magnetohydrodynamic (MHD) setting; see, e.g., [2]. In the kinetic framework, a numerical investigation of the classical VP system in the 1D1V setting using an externally applied electric field was carried out in [23]. Related numerical studies include [24–27], where control is achieved via externally applied magnetic fields. These numerical works were followed by the theoretical development in [28], which introduced the pole-elimination strategy as a general mechanism for suppressing instability. Building on this idea, we develop a pole-elimination-based control design for the magnetized Vlasov–Poisson system (1.1). Our construction uses a detailed analysis of the associated dispersion relation to derive an explicit feedback term H that removes the unstable spectral contributions (i.e., modes with positive growth rates) and thereby stabilizes the dynamics. While conceptually inspired by [28], the present setting introduces substantial new technical challenges: the analysis is

carried out in the full 3D3V phase space and must account for the anisotropic geometry induced by a strong external magnetic field, including the distinguished role of the x_3 -direction. This leads to new phenomena absent in the unmagnetized case, such as the treatment of ring-type equilibria and the presence of Bernstein modes ($k_3 = 0$), both of which require additional structural considerations in the control design and stability analysis. We also note that this direction differs from work on magnetic confinement [9–11], which focuses on maintaining spatial confinement, instead of stability, of the plasma in bounded geometries under external fields.

The paper is organized as follows. In Section 2 we provide linear stability analysis, and derive the Penrose condition and dispersion relation for our system. This provides the baseline for understanding the stability of the system without control. Our control strategies are then provided in Section 3. The Penrose condition reveals the structure of instability, and our control strategies target eliminating the growing modes. One control further recovers the free-streaming solution. Numerical evidences are provided in Section 4.

2 Linear analysis

In this section, we derive the generalized Penrose condition and the dispersion relation of system (1.1) in section 2.1. This set of analytical derivations provides us with insights into the possibility of plasma generating instability. It will be followed in section 2.2 by two case studies with two different equilibrium states: Gaussian equilibrium and ring-shaped distribution, in which we apply the previously obtained generalized Penrose condition to evaluate the stability of the system.

Before we conduct linearization, we lay out a few important properties of the system and its equilibrium states in the following proposition.

Proposition 2.1 *Vlasov-Poisson system with external magnetic field (1.1) satisfies the following properties:*

- Any function of the following form is an equilibrium to (1.1):

$$\mu(\mathbf{v}) \propto \mu_{\perp} \left(\sqrt{v_1^2 + v_2^2} \right) \mu_{\parallel}(v_3),$$

This includes the standard Gaussian distribution or anisotropic Gaussian with different temperatures for \mathbf{v}_{\perp} and v_3 .

- The Vlasov-Poisson system (1.1) conserves total energy,

$$\mathcal{E}_{total} := \frac{1}{2} \int |\mathbf{v}|^2 F(t, \mathbf{x}, \mathbf{v}) d\mathbf{v} d\mathbf{x} + \frac{1}{2} \int |\mathbf{E}|^2(t, \mathbf{x}) d\mathbf{x},$$

and the second term is the electric energy:

$$\mathcal{E}(t) := \frac{1}{2} \int |\mathbf{E}|^2(t, \mathbf{x}) d\mathbf{x}. \quad (2.1)$$

The proof for the proposition is standard material and is omitted from here. It is also worth noting that the \mathbf{B} -component of the acceleration is $\mathbf{v} \times \mathbf{B}$, and this component preserves the magnetic moment $\frac{v_{\perp}^2}{2B_0}$.

For any given equilibrium $\mu(\mathbf{v})$ of (1.1), we consider a small perturbation around the equilibrium, i.e., $F := \mu(\mathbf{v}) + f$. The perturbation solves the linearized magnetized Vlasov-Poisson system:

$$\partial_t f + \mathbf{v} \cdot \nabla_{\mathbf{x}} f + (v_2 B_0 \partial_{v_1} f - v_1 B_0 \partial_{v_2} f) + \mathbf{E} \cdot \nabla_{\mathbf{v}} \mu(\mathbf{v}) = 0, \quad \mathbf{x} \in \mathbb{T}^3, \mathbf{v} \in \mathbb{R}^3 \quad (2.2)$$

$$\nabla_{\mathbf{x}}^2 U = - \int_{\mathbb{R}^3} f d\mathbf{v}, \quad (2.3)$$

$$\mathbf{E} = -\nabla_{\mathbf{x}} U. \quad (2.4)$$

The system is equipped with initial data $f(t = 0, \cdot, \cdot) = f_0$. It is on this linearized equation that we conduct studies on the dispersion relation.

2.1 Stability condition.

We first perform the derivation of the dispersion relation for (2.2). The technique has been deployed in [22] for Vlasov-Poisson, a slightly simpler system.

To do so, we are to denote the Fourier transform of $f(t, \mathbf{x}, \mathbf{v})$ of phase space as

$$\hat{f}(t, \mathbf{k}, \mathbf{m}) := \int_{\mathbb{T}^3} \int_{\mathbb{R}^3} e^{-i\mathbf{k} \cdot \mathbf{x} - i\mathbf{m} \cdot \mathbf{v}} f(t, \mathbf{x}, \mathbf{v}) d\mathbf{x} d\mathbf{v}, \quad \mathbf{k} \in \mathbb{Z}^3, \mathbf{m} \in \mathbb{R}^3,$$

and the Laplace transform $f(t)$ in time t as

$$L[f](\lambda) := \int_0^{\infty} e^{-\lambda t} f(t) dt, \quad \lambda \in \mathbb{C}.$$

The dispersion relation is summarized in the following proposition.

Proposition 2.2 (Penrose condition) *The VP system (2.2) in Laplace-Fourier space translates to:*

$$P(\mathbf{k}, \lambda) L[\hat{U}] = L[\hat{S}], \quad \forall \mathbf{k} \in \mathbb{Z}^3, \lambda \in \mathbb{C} \quad (2.5)$$

where $P(\mathbf{k}, \lambda)$ is:

$$P(\mathbf{k}, \lambda) = \mathbf{k} \cdot (I + L[\hat{\rho} \tilde{\mathbf{R}}](\lambda, \mathbf{k})) \mathbf{k}, \quad (2.6)$$

U is the self-generating electric potential, and

- S is the free streaming density defined as:

$$S(t, \mathbf{x}) = \int f_0(\mathbf{y}^{-1}(t; \mathbf{x}, \mathbf{v}), \mathbf{u}^{-1}(t; \mathbf{v})) d\mathbf{v}, \quad (2.7)$$

where $(\mathbf{y}(t; \mathbf{x}, \mathbf{v}), \mathbf{u}(t; \mathbf{v}))$ denotes the position and velocity of a particle following characteristics of the VP system with initial data at (\mathbf{x}, \mathbf{v}) , see explicit calculation in (2.14), and f_0 denotes the initial condition.

$$\tilde{\mathbf{R}}(t) := \begin{pmatrix} \frac{1}{B_0} (\mathbf{R}(\frac{\pi}{2} - B_0 t) - \mathbf{R}(\frac{\pi}{2})) & 0 \\ 0 & t \end{pmatrix}, \quad \text{where } \mathbf{R}(\alpha) := \begin{pmatrix} \cos(\alpha) & \sin(\alpha) \\ -\sin(\alpha) & \cos(\alpha) \end{pmatrix}. \quad (2.8)$$

Furthermore, if there exists some $\kappa_0 > 0$ that

$$\inf_{\mathbf{k} \in \mathbb{Z}^3, \operatorname{Re}(\lambda) > 0} |\mathbf{k} \cdot (I + L[\hat{\mu}\tilde{\mathbf{R}}](\lambda, \mathbf{k}))\mathbf{k}| \geq \kappa_0, \quad (2.9)$$

then the equilibrium μ is stable, in the sense that electric energy $\mathcal{E}(t)$ does not blow up.

Remark 2.1 It is straightforward to see (2.5) is an extension from the VP system without the external field. Indeed, without the \mathbf{B} , one has the same equation that writes:

$$P(\mathbf{k}, \lambda)L[\hat{U}] = L[\hat{S}] \quad \text{with } P(\mathbf{k}, \lambda) = \mathbf{k} \cdot (I + L[t\hat{\mu}(\lambda, \mathbf{k}t)])\mathbf{k} \quad (2.10)$$

In comparison to (2.10), our equation (2.5) has the same right-hand side that is also generated by the free-streaming solution, and our dispersion function P now involves the rotational operator (2.8). This rotation is a natural consequence of the gyro-effect induced by \mathbf{B} .

Complementary to the Penrose condition (2.9), suppose that there exist $\mathbf{k} \in \mathbb{Z}^3$ and $\lambda_0 \in \mathbb{C}$ such that $P(\mathbf{k}, \lambda_0) = 0$, then the temporal behavior of the corresponding mode is characterized by the complex root λ_0 . In particular, the real part of λ_0 , $\operatorname{Re}(\lambda_0)$, determines whether the mode grows, decays, or remains neutral in time. If $\operatorname{Re}(\lambda_0) = 0$, the associated electric energy does not grow or decay and corresponds to a neutrally stable mode. If $\operatorname{Re}(\lambda_0) > 0$, the mode exhibits exponential growth in time, indicating a potential instability.

Before proving the proposition, we first prepare the free-streaming solution and characteristics of (2.2). Setting the free-streaming component of the equation

$$\partial_t f_{\mathbf{f}} + \mathbf{v} \cdot \nabla_{\mathbf{x}} f_{\mathbf{f}} + (\mathbf{v} \times \mathbf{B}) \cdot \nabla_{\mathbf{v}} f_{\mathbf{f}} = 0, \quad (2.11)$$

we notice that

$$\frac{d}{dt} \mathbf{y}(t) = \mathbf{u}(t), \quad (2.12)$$

$$\frac{d}{dt} \mathbf{u}(t) = \begin{pmatrix} 0 & B_0 & 0 \\ -B_0 & 0 & 0 \\ 0 & 0 & 0 \end{pmatrix} \mathbf{u}(t). \quad (2.13)$$

For this linear ODE system, the solution is explicit — the celebrated the Larmour trajectory (rotation) :

$$\begin{pmatrix} \mathbf{u}_{\perp}(t) \\ u_3(t) \end{pmatrix} = \begin{pmatrix} \mathbf{R}(B_0 t) & 0 \\ 0 & 1 \end{pmatrix} \begin{pmatrix} \mathbf{v}_{\perp} \\ v_3 \end{pmatrix}, \quad (2.14)$$

$$\begin{pmatrix} \mathbf{y}_\perp(t) \\ y_3(t) \end{pmatrix} = \begin{pmatrix} \mathbf{x}_\perp \\ x_3 \end{pmatrix} + \begin{pmatrix} \mathbf{M}(t) + \mathbf{Q} & 0 \\ 0 & t \end{pmatrix} \begin{pmatrix} \mathbf{v}_\perp \\ v_3 \end{pmatrix}. \quad (2.15)$$

where \mathbf{M} and \mathbf{Q} are auxiliary matrices defined by:

$$\mathbf{M}(t) := \frac{1}{B_0} \mathbf{R} \left(B_0 t - \frac{\pi}{2} \right) = \frac{1}{B_0} \begin{pmatrix} \sin(B_0 t) & -\cos(B_0 t) \\ \cos(B_0 t) & \sin(B_0 t) \end{pmatrix}, \quad \mathbf{Q} := \frac{1}{B_0} \begin{pmatrix} 0 & 1 \\ -1 & 0 \end{pmatrix}.$$

As a consequence,

$$f_{\mathbf{f}}(t, \mathbf{x}, \mathbf{v}) = f_0(\mathbf{x}_\perp - (\mathbf{M}(t) + \mathbf{Q})\mathbf{R}^{-1}(B_0 t)\mathbf{v}_\perp, x_3 - v_3 t, \mathbf{R}^{-1}(B_0 t)\mathbf{v}_\perp, v_3). \quad (2.16)$$

and

$$S(t, x) = \int f_{\mathbf{f}}(t; \mathbf{x}, \mathbf{v}) d\mathbf{v},$$

recovering (2.7). Moreover, define

$$g(t, \mathbf{x}, \mathbf{v}) := f(t, \mathbf{y}(t; \mathbf{x}, \mathbf{v}), \mathbf{u}(t; \mathbf{v})),$$

we have, by plugging in the linearized equation of f (2.2):

$$\begin{aligned} \frac{dg}{dt}(t, \mathbf{x}, \mathbf{v}) &= \partial_t f + \frac{d\mathbf{y}}{dt} \cdot \nabla_{\mathbf{x}} f + \frac{d\mathbf{u}}{dt} \cdot \nabla_{\mathbf{v}} f, \\ &= \partial_t f + \mathbf{u}(t) \cdot \nabla_{\mathbf{x}} f + B_0 u_2 \partial_{v_1} f - B_0 u_1 \partial_{v_2} f \\ &= -\mathbf{E}(\mathbf{y}(t; \mathbf{x}, \mathbf{v})) \cdot \nabla_{\mathbf{v}} \mu(\mathbf{u}(t; \mathbf{v})). \end{aligned} \quad (2.17)$$

Proposition 2.2 is proved by conducting a Laplace-Fourier transform of equation (2.17).

Proof of Proposition 2.2 We first notice there are two equations connecting g and \mathbf{E} , one by (2.17), and the second by the definition of electric field:

$$\nabla_{\mathbf{x}} \cdot \mathbf{E}(t, \mathbf{x}) = \int_{\mathbb{R}^3} f(t, \mathbf{x}, \mathbf{v}) d\mathbf{v} = \rho(t, \mathbf{x}).$$

We need to flip both equations to the Fourier side. The Fourier transform of the Poisson equation is straightforward. By definition,

$$f(t, \mathbf{x}, \mathbf{v}) = g(t; \mathbf{x}_\perp - (\mathbf{M}(t) + \mathbf{Q})\mathbf{R}(B_0 t)^{-1}\mathbf{v}_\perp, x_3 - v_3 t, \mathbf{R}(B_0 t)^{-1}\mathbf{v}_\perp, v_3). \quad (2.18)$$

So

$$\begin{aligned} i\mathbf{k} \cdot \hat{E}(t, \mathbf{k}) &= \hat{\rho}(t, \mathbf{k}) = \int_{\mathbb{T}^3} \int_{\mathbb{R}^3} e^{-i\mathbf{k} \cdot \mathbf{x}} f(t, \mathbf{x}, \mathbf{v}) d\mathbf{v} d\mathbf{x}, \\ &= \int_{\mathbb{T}^3} \int_{\mathbb{R}^3} e^{-i\mathbf{k} \cdot \mathbf{x}} g(t; \mathbf{x}_\perp - (\mathbf{M}(t) + \mathbf{Q})\mathbf{R}(B_0 t)^{-1}\mathbf{v}_\perp, x_3 - v_3 t, \mathbf{R}(B_0 t)^{-1}\mathbf{v}_\perp, v_3) d\mathbf{v} d\mathbf{x}, \\ &= \int_{\mathbb{T}^3} \int_{\mathbb{R}^3} e^{-i\mathbf{k}_\perp \cdot (\mathbf{x}_\perp - (\mathbf{M}(t) + \mathbf{Q})\mathbf{R}(B_0 t)^{-1}\mathbf{v}_\perp)} e^{-ik_3(x_3 - v_3 t)} e^{-i(\mathbf{M}(t) + \mathbf{Q})\mathbf{R}(B_0 t)^{-1}\mathbf{v}_\perp} e^{-ik_3 t v_3} \\ &\quad g(t; \mathbf{x}_\perp - (\mathbf{M}(t) + \mathbf{Q})\mathbf{R}(B_0 t)^{-1}\mathbf{v}_\perp, x_3 - v_3 t, \mathbf{R}(B_0 t)^{-1}\mathbf{v}_\perp, v_3) d\mathbf{v} d\mathbf{x}, \\ &= \hat{g}(t, \mathbf{k}_\perp, k_3, (\mathbf{M}(t) + \mathbf{Q})^\top \mathbf{k}_\perp, k_3 t), \end{aligned} \quad (2.19)$$

where we used a change of variable.

Similarly, we conduct the Fourier transform on (\mathbf{x}, \mathbf{v}) of (2.17). Denoting \mathbf{k} and \mathbf{m} the associated Fourier coefficients, the equation becomes:

$$\begin{aligned}
\frac{d\hat{g}}{dt}(t, \mathbf{k}, \mathbf{m}) &= - \int_{\mathbb{T}^3} \int_{\mathbb{R}^3} e^{-i\mathbf{k}\cdot\mathbf{x} - i\mathbf{m}\cdot\mathbf{v}} \mathbf{E}(\mathbf{y}(t; \mathbf{x}, \mathbf{v})) \cdot \nabla_{\mathbf{v}} \mu(\mathbf{u}(t; \mathbf{v})) \, d\mathbf{x} d\mathbf{v}, \\
&= - \int_{\mathbb{T}^3} \int_{\mathbb{R}^3} e^{-i\mathbf{k}\cdot\mathbf{x} - i\mathbf{m}\cdot\mathbf{v}} \mathbf{E}(\mathbf{x}_{\perp} + (\mathbf{M}(t) + \mathbf{Q})\mathbf{v}_{\perp}, x_3 + v_3 t) \cdot \nabla_{\mathbf{v}} \mu(\mathbf{R}(B_0 t)\mathbf{v}_{\perp}, v_3) \, d\mathbf{x} d\mathbf{v}, \\
&= - \hat{\mathbf{E}}(t, \mathbf{k}) \cdot \int_{\mathbb{R}^3} e^{+i\mathbf{k}_{\perp} \cdot (\mathbf{M}(t) + \mathbf{Q})\mathbf{v}_{\perp} + ik_3 v_3 t - i\mathbf{m}\cdot\mathbf{v}} \nabla_{\mathbf{v}} \mu(\mathbf{R}(B_0 t)\mathbf{v}_{\perp}, v_3) \, d\mathbf{x} d\mathbf{v}, \\
&= - i \begin{pmatrix} \hat{\mathbf{E}}_{\perp}(t, \mathbf{k}) \\ \hat{E}_3(t, \mathbf{k}) \end{pmatrix} \cdot \begin{pmatrix} \mathbf{R}(B_0 t)(\mathbf{m}_{\perp} - (\mathbf{M}(t) + \mathbf{Q})^{\top} \mathbf{k}_{\perp}) \\ m_3 - k_3 t \end{pmatrix} \\
&\quad \hat{\mu}(\mathbf{R}(B_0 t)(\mathbf{m}_{\perp} - (\mathbf{M}(t) + \mathbf{Q})^{\top} \mathbf{k}_{\perp}), m_3 - k_3 t). \tag{2.20}
\end{aligned}$$

This equation holds for all values of (\mathbf{k}, \mathbf{m}) . We choose a special pair. Let $\mathbf{m} = (\mathbf{m}_{\perp}, m_3)$ defined by:

$$\mathbf{m}_{\perp}(\mathbf{k}) := (\mathbf{M}(t) + \mathbf{Q})^{\top} \mathbf{k}_{\perp}, \quad m_3(\mathbf{k}) := k_3 t, \tag{2.21}$$

then for $0 < s < t$,

$$\begin{aligned}
\mathbf{R}(B_0 s)(\mathbf{m}_{\perp}(\mathbf{k}) - (\mathbf{M}(s) + \mathbf{Q})^{\top} \mathbf{k}_{\perp}) &= \mathbf{R}(B_0 s)(\mathbf{M}(t) - \mathbf{M}(s))^{\top} \mathbf{k}_{\perp} \\
&= \frac{1}{B_0} \left(\mathbf{R}\left(\frac{\pi}{2} - B_0(t-s)\right) - \mathbf{R}\left(\frac{\pi}{2}\right) \right) \mathbf{k}_{\perp}.
\end{aligned}$$

Integrate (2.20) in time for this specifically chosen $(\mathbf{k}, \mathbf{m}(\mathbf{k}))$, and recall the definition of $\tilde{\mathbf{R}}$ in (2.8), we have:

$$\hat{g}(t, \mathbf{k}, \mathbf{m}(\mathbf{k})) - \hat{g}(0, \mathbf{k}, \mathbf{m}(\mathbf{k})) + i \int_0^t \begin{pmatrix} \hat{\mathbf{E}}_{\perp}(s, \mathbf{k}) \\ \hat{E}_3(s, \mathbf{k}) \end{pmatrix} \cdot \tilde{\mathbf{R}}(t-s) \begin{pmatrix} \mathbf{k}_{\perp} \\ k_3 \end{pmatrix} \hat{\mu}(\tilde{\mathbf{R}}(t-s)\mathbf{k}) \, ds = 0. \tag{2.22}$$

We are going to apply the Laplace transform on all three terms by multiplying $e^{-\lambda t}$ and integrating in t -dimension.

– By (2.19), the first term

$$\hat{g}(t, \mathbf{k}, \mathbf{m}(\mathbf{k})) = i\mathbf{k} \cdot \hat{\mathbf{E}}(t, \mathbf{k}).$$

Hence, using the linearity of the Laplace transform operator, the first term becomes: $i\mathbf{k} \cdot L[\hat{\mathbf{E}}]$;

– By definition of free-streaming (2.16), $\hat{f}_f = \hat{f}_0(\mathbf{k}, \mathbf{m}(\mathbf{k})) = \hat{g}(0, \mathbf{k}, \mathbf{m}(\mathbf{k}))$, and with the same calculation as done in (2.19), the second term becomes: $L[\hat{S}]$;

– To compute the last term, we notice it has the convolution structure between $\hat{\mu}\tilde{\mathbf{R}}$ and $\hat{\mathbf{E}}$, the Laplace transform thus becomes:

$$\begin{aligned}
&\int_0^{\infty} \int_0^t e^{-\lambda t} \begin{pmatrix} \hat{\mathbf{E}}_{\perp}(s, \mathbf{k}) \\ \hat{E}_3(s, \mathbf{k}) \end{pmatrix} \cdot \tilde{\mathbf{R}}(t-s) \begin{pmatrix} \mathbf{k}_{\perp} \\ k_3 \end{pmatrix} \hat{\mu}(\tilde{\mathbf{R}}(t-s)\mathbf{k}) \, ds dt, \\
&= \int_0^{\infty} \int_0^{\infty} e^{-\lambda w} e^{-\lambda s} \begin{pmatrix} \hat{\mathbf{E}}_{\perp}(s, \mathbf{k}) \\ \hat{E}_3(s, \mathbf{k}) \end{pmatrix} \cdot \tilde{\mathbf{R}}(w) \begin{pmatrix} \mathbf{k}_{\perp} \\ k_3 \end{pmatrix} \hat{\mu}(\tilde{\mathbf{R}}(w)\mathbf{k}) \, dw ds, \quad (w := t-s),
\end{aligned}$$

$$= \int_0^\infty e^{-\lambda s} \begin{pmatrix} \hat{E}_\perp(s, \mathbf{k}) \\ \hat{E}_3(s, \mathbf{k}) \end{pmatrix} ds \cdot \int_0^\infty e^{-\lambda t} \tilde{\mathbf{R}}(t) \hat{\mu}(\tilde{\mathbf{R}}(t)\mathbf{k}) dt \begin{pmatrix} \mathbf{k}_\perp \\ k_3 \end{pmatrix} \quad (2.23)$$

$$= L[\hat{\mathbf{E}}] \cdot L[\hat{\mu}\tilde{\mathbf{R}}]\mathbf{k}. \quad (2.24)$$

Putting these three terms together in (2.22), we have

$$i\mathbf{k} \cdot L[\hat{\mathbf{E}}] - L[\hat{S}] + iL[\hat{\mathbf{E}}] \cdot L[\hat{\mu}\tilde{\mathbf{R}}]\mathbf{k} = 0. \quad (2.25)$$

Noting the relation between \mathbf{E} and U :

$$-|\mathbf{k}|^2 \hat{U}(t, \mathbf{k}) = -\hat{\rho}(t, \mathbf{k}), \quad \Rightarrow \quad \hat{\mathbf{E}} = -i\mathbf{k}\hat{U} = -i\frac{\mathbf{k}}{|\mathbf{k}|^2} \hat{\rho}(t, \mathbf{k}),$$

we rewrite (2.25) into:

$$\left(\mathbf{k} \cdot \left(I + L[\hat{\mu}\tilde{\mathbf{R}}] \right) \mathbf{k} \right) L[\hat{U}] = L[\hat{S}], \quad (2.26)$$

hence proving (2.5). The stability condition (2.9) comes from inverting the Laplace transform [29]. \square

2.2 Two case studies

In this subsection, we compute (2.6) for two equilibria, the Gaussian equilibrium and a ring-shaped equilibrium that generates Dory-Guest-Harris instability. Moreover, we restrict ourselves to the Bernstein modes, the Fourier modes of $\mathbf{k} = (k_1, k_2, 0)^\top$ that are transverse to the magnetic field. Consequently, the derivation of the rest of the paper is conducted in $2D2V$.

Remark 2.2 For another specific mode in the form of $(0, 0, k_3)^\top$, our linear analysis recovers the previous results of Vlasov-Poisson [28], where $\mu_\parallel(v_3)$ is two-stream instability or bump-on-tail instability along the magnetic field direction.

2.2.1 Gaussian equilibrium.

We first consider Gaussian equilibrium of (2.2). The Gaussian equilibrium has been proved to have non-decaying electric energy for Bernstein modes [12]. That is, for each $\mathbf{k} = (k_1, k_2)^\top \in \mathbb{Z}^2$, the poles of $P(\mathbf{k}, \lambda)$ are located along the imaginary line.

Let μ be any isotropic Gaussian distribution on $(v_1, v_2)^\top$, i.e.

$$\mu(\mathbf{v}) = \frac{1}{2\pi\theta} e^{-\frac{v_1^2 + v_2^2}{2\theta}}. \quad (2.27)$$

According to (2.6),

$$\begin{aligned} P(\mathbf{k}, \lambda) &= |\mathbf{k}|^2 + |\mathbf{k}|^2 \frac{1}{B_0} \int_0^\infty e^{-\lambda t} \hat{\mu}(\tilde{\mathbf{R}}(t)\mathbf{k}) \sin(B_0 t) dt, \\ &= |\mathbf{k}|^2 \left(1 + \frac{1}{B_0} \int_0^\infty e^{-\lambda t} \exp\left(-\frac{\theta}{B_0^2} (1 - \cos(B_0 t)) |\mathbf{k}|^2\right) \sin(B_0 t) dt \right), \end{aligned}$$

where we used:

$$\mathbf{k} \cdot \tilde{\mathbf{R}}(t) \mathbf{k} = \begin{pmatrix} k_1 \\ k_2 \end{pmatrix}^\top \frac{1}{B_0} \begin{pmatrix} \sin(B_0 t) & \cos(B_0 t) - 1 \\ -\cos(B_0 t) + 1 & \sin(B_0 t) \end{pmatrix} \begin{pmatrix} k_1 \\ k_2 \end{pmatrix} = \frac{\sin(B_0 t)}{B_0} |\mathbf{k}|^2.$$

In the following we set $\theta = 1$, $B_0 = 1$ and $\mathbf{k}_\perp = (1, 0)^\top$ without loss of generality, then

$$P(\mathbf{k}, \lambda) = 1 + \int_0^\infty e^{-\lambda t} e^{-1+\cos(t)} \sin(t) dt,$$

In Figure 1, we plot the equilibrium (2.27) and the evaluation of $P(\mathbf{k}, \lambda)$ for $\lambda = \text{Re}(\lambda) + i\text{Im}(\lambda)$ with $(\text{Re}(\lambda), \text{Im}(\lambda)) \in [0.001, 0.1] \times [1.05, 1.25]$. Since poles for P are complex conjugate pairs, we only plot them on the $\text{Im}(\lambda) > 0$. The plot shows that we can numerically find a root at $(\text{Re}\lambda = 0.001, \text{Im}(\lambda) = 1.164)$. This is consistent with the analytical prediction in [12] that suggests all roots should be along the imaginary line¹.

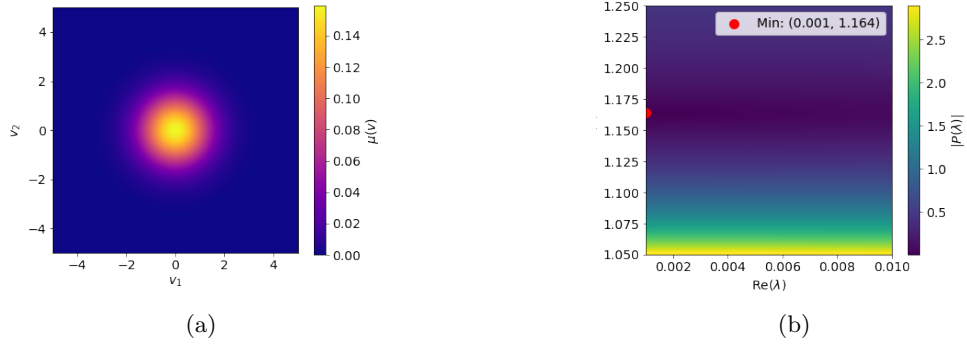


Fig. 1: Isotropic Gaussian μ and $|P(\mathbf{k}, \lambda)|$. The minimum is taken at $(\text{Re}(\lambda) = 0.001, \text{Im}(\lambda) = 1.164)$ with value $\min |P(0.001, 1.164)| = 2 \times 10^{-3}$.

2.2.2 Dory-Guest-Harris instability

We also demonstrate the computation of (2.6) for the ring-shaped equilibrium as discussed in [13],

$$\mu(\mathbf{v}) = \frac{1}{\pi \alpha_\perp^2 j!} \left(\frac{v_1^2 + v_2^2}{\alpha_\perp^2} \right)^j \exp\left(-\frac{v_1^2 + v_2^2}{\alpha_\perp^2}\right). \quad (2.28)$$

¹Numerically, we cannot compute $P(\mathbf{k}, \lambda)$ for $\text{Re}(\lambda) = 0$.

A special case for this equilibrium is when $j = 0$, when it recovers the Gaussian equilibrium. It was further identified [13] the equilibrium (2.28) continue being unconditionally stable for $j \in \{0, 1, 2\}$. However, for $j \geq 3$, the equilibrium (2.28) can be unstable, and this instability is termed the Dory-Guest-Harris instability. Intuitively, for larger j , the distribution becomes more concentrated on a ring [30, 31], and this concentration leads to instability. The cases of $j = 3, 4, 5, 6$ were thoroughly studied in [15].

We leave detailed derivation to Appendix A.1. In the following example we set $j = 6, \alpha_{\perp} = \sqrt{1/3}, B_0 = 0.05$, then

$$\mu(\mathbf{v}) = \frac{3}{\pi 6!} \left(\frac{v_1^2 + v_2^2}{1/3} \right)^6 \exp\left(-\frac{v_1^2 + v_2^2}{1/3}\right). \quad (2.29)$$

In this case, according to the derivation in Appendix A.1, we have

$$P(\mathbf{k}, \lambda) = |\mathbf{k}|^2 \left(1 + \int_0^{\infty} \exp(-\lambda t - z) M(-6, 1, z) \frac{\sin(B_0 t)}{B_0} dt \right).$$

where $z = \frac{1}{6B_0^2} |\mathbf{k}|^2 (1 - \cos(B_0 t))$.

Again without loss of generality, we fix $|\mathbf{k}|^2 = 1$, i.e. $\mathbf{k} = (1, 0)^{\top}$ or $\mathbf{k} = (0, 1)^{\top}$, and numerically compute P as a function of λ (2.9). In Figure 2 we plot both the distribution function (2.29) and $P(\mathbf{k} = (1, 0), \lambda)$. Clearly, in this case, we find a root with a positive real component, indicating the instability of this equilibrium.

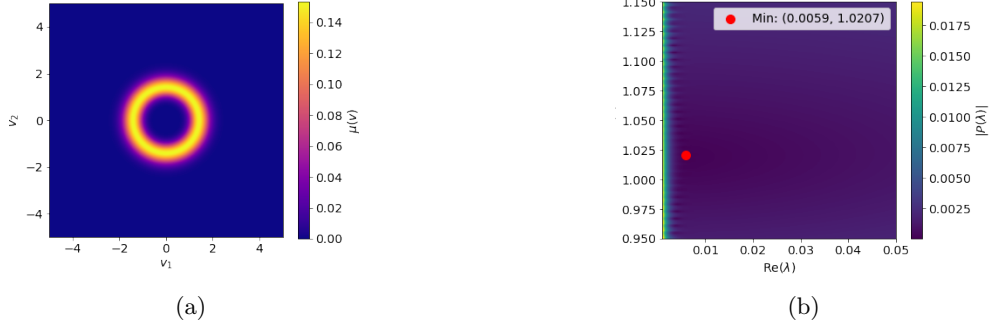


Fig. 2: Equilibrium distribution (2.29) and $|P(\mathbf{k}, \lambda)|$ (2.6). The minimum is taken at $(\lambda_R = 0.0059, \lambda_I = 1.0207)$ with minimal value 1.5×10^{-5} .

3 Control with an external electric field

Our strategy to suppress instability in the magnetized Vlasov-Poisson system is to add an external electric field. Add an external electric field $-\nabla_{\mathbf{x}}\Phi(t, \mathbf{x})$, generated by

some electric potential Φ , to the system (2.2), the system is:

$$\partial_t f + \mathbf{v} \cdot \nabla_{\mathbf{x}} f + (v_2 B_0 \partial_{v_1} f - v_1 B_0 \partial_{v_2} f) + (\mathbf{E} - \nabla_{\mathbf{x}} \Phi) \cdot \nabla_{\mathbf{v}} \mu(\mathbf{v}) = 0, \quad (3.1)$$

$$\nabla_{\mathbf{x}} \cdot \mathbf{E} = \int_{\mathbb{R}^3} f d\mathbf{v}. \quad (3.2)$$

Following the same linear analysis as in Proposition 2.2, we have:

$$|\mathbf{k}|^2 L[\hat{U}] - L[\hat{S}] + (L[\hat{U}] + L[\hat{\Phi}]) \mathbf{k} \cdot L[\hat{\mu} \tilde{R}] \mathbf{k} = 0, \quad (3.3)$$

where we used $\hat{\mathbf{E}} = -i\mathbf{k}\hat{U}$. Notice $1 = \frac{\mathbf{k} \cdot \mathbf{k}}{|\mathbf{k}|^2}$ and recall the definition of our dispersion function (2.6), the equation becomes:

$$P(\mathbf{k}, \lambda) L[\hat{U}] = L[\hat{S}] - L[\hat{\Phi}] \mathbf{k} \cdot L[\hat{\mu} \tilde{R}] \mathbf{k}. \quad (3.4)$$

Compare this equation with (2.5), we quickly notice that the only difference is that the right-hand side is modified with a new source term that depends on the external potential Φ . Physically, one could wish to have the solution to be close to the free-streaming, which requires U , the self-generated electric field, to satisfy $\Delta U = S$. For computational convenience, it would be easier to translate the equation into:

$$P(\mathbf{k}, \lambda) \left(|\mathbf{k}|^2 L[\hat{U}] - L[\hat{S}] \right) = - \left(|\mathbf{k}|^2 L[\hat{\Phi}] + L[\hat{S}] \right) \mathbf{k} \cdot L[\hat{\mu} \tilde{R}] \mathbf{k}, \quad (3.5)$$

Recall Proposition 2.2, instability is observed when P has roots on $\text{Re}(\lambda) > 0$ side of the plane. One straightforward strategy to eliminate this instability is to set Φ so to have the entire source term in (3.5) cancels out the roots of P . Mathematically, this is to set:

$$\lim_{\lambda \rightarrow \lambda_0} \frac{\left(|\mathbf{k}|^2 L[\hat{\Phi}] + L[\hat{S}] \right) \mathbf{k} \cdot L[\hat{\mu} \tilde{R}] \mathbf{k}}{P(\mathbf{k}, \lambda)} = c, \quad \forall \mathbf{k}, \lambda_0 \quad \text{s.t.} \quad P(\mathbf{k}, \lambda_0) = 0. \quad (3.6)$$

The constant c here can be arbitrary. Since we do not have control over $\mathbf{k} \cdot L[\hat{\mu} \tilde{R}] \mathbf{k}$, the control strategy becomes manipulating $|\mathbf{k}|^2 L[\hat{\Phi}] + L[\hat{S}]$ only. In the subsequent two sections, we propose two simplest options to achieve (3.6).

3.1 Control Strategy 1: set $c \equiv 0$ in (3.6).

This, according to (3.6), leads to:

$$|\mathbf{k}|^2 L[\hat{\Phi}] + L[\hat{S}] = 0, \quad \forall \mathbf{k} \in \mathbb{Z}^3, \lambda. \quad (3.7)$$

Take the inverse Laplace transform and the inverse Fourier transform, and this requirement becomes

$$-\Delta \Phi = S,$$

where S is defined as in (2.7). When (3.7) holds, the right hand side of (3.5) is zero, and we will also obtain:

$$\Delta U = S.$$

This means the self-generated electric field is completely zeroed out by the external field $\nabla_{\mathbf{x}}\Phi$. Plugging them in (3.1), we find the solution recovers the free-streaming solution, as described in the following lemma.

Lemma 3.1 *The controlled system (3.1) with Φ designed in (3.7) coincides with the free-streaming solution (2.11) for all time.*

Proof Define the difference of solution $f_\delta = f - f_f$, and we obtain the system of f_δ by subtracting (3.1) from (2.11):

$$\partial_t f_\delta + \mathbf{v} \cdot \nabla_{\mathbf{x}} f_\delta + (\mathbf{v} \times \mathbf{B}) \cdot \nabla_{\mathbf{v}} f_\delta + (\mathbf{E}[f] - \nabla_{\mathbf{x}}\Phi) \cdot \nabla_{\mathbf{v}} \mu = 0, \quad (3.8)$$

$$f_\delta(t=0, \mathbf{x}, \mathbf{v}) = 0. \quad (3.9)$$

Using the linearity of \mathbf{E} , we compute

$$\mathbf{E}[f] - \nabla_{\mathbf{x}}\Phi = \mathbf{E}[f] - \mathbf{E}[f_f] = \mathbf{E}[f_\delta](t, \mathbf{x}).$$

The system is thus linear in f_δ . Since the initial data is 0, the solution is always zero: $f_\delta \equiv 0$. \square

Remark 3.1 *We should note that this control strategy is also effective for the nonlinear Vlasov-Poisson system. Indeed, by revising (3.1) into:*

$$\partial_t f + \mathbf{v} \cdot \nabla_{\mathbf{x}} f + (v_2 B_0 \partial_{v_1} f - v_1 B_0 \partial_{v_2} f) + (\mathbf{E} - \nabla_{\mathbf{x}}\Phi) \cdot \nabla_{\mathbf{v}} f = 0.$$

Setting $\Phi = U$, we still recover the free-streaming solution for all time.

By linking the controlled system (3.1) with the free-streaming solution, we can explicitly analyze the in-time dynamics of the electric energy.

Theorem 3.1 *Let f be the solution to (3.1) with the external field prepared in (3.7), equipped with separable initial profile: $f_0(\mathbf{x}, \mathbf{v}) = \chi(\mathbf{x})\mu(\mathbf{v})$ where $\mu(\mathbf{v})$ is Gaussian with temperature θ , and $\chi(\mathbf{x})$ is periodic in space and $\hat{\chi}$ is bounded. Denote \mathcal{E} as the electric energy defined in (2.1). Let $\mathcal{E}_{\mathbf{k}}(t) := \frac{1}{2}|\hat{\mathbf{E}}(t, \mathbf{k})|^2$ be the $\mathbf{k} = (k_1, k_2, k_3)$ -th mode of \mathcal{E} . Then:*

- *For non-Bernstein modes, i.e. $k_3 \neq 0$, electric energy $\mathcal{E}_{\mathbf{k}}(t)$ exponentially decays in time.*
- *For Bernstein modes, i.e. $k_3 = 0$, electric energy $\mathcal{E}_{\mathbf{k}}(t)$ presents a periodic pattern in time with the period being $\frac{2\pi}{B_0}$, the inverse of the standard gyrofrequency in plasma physics.*

This theorem suggests, in the long time, the electric energy is predominantly governed by modes perpendicular to \mathbf{B} .

Proof According to Lemma 3.1, the controlled solution recovers the free-streaming solution, and thus, recall (2.16):

$$f(t, \mathbf{x}, \mathbf{v}) = f_f(t, \mathbf{x}, \mathbf{v}) = \chi(\mathbf{x}_\perp - (\mathbf{M}(t) + \mathbf{Q})\mathbf{R}^{-1}(B_0 t)\mathbf{v}_\perp, x_3 - v_3 t)\mu(\mathbf{R}^{-1}(B_0 t)\mathbf{v}_\perp, v_3).$$

Take the Fourier transform and integrate in the velocity space:

$$\begin{aligned} \hat{\rho}(t, \mathbf{k}) &= \int e^{-i\mathbf{k}\cdot\mathbf{x}} \int f(t, \mathbf{x}, \mathbf{v}) d\mathbf{v} d\mathbf{x}, \\ &= \int e^{-i\mathbf{k}\cdot\mathbf{x}} \int \chi(\mathbf{x}_\perp - (\mathbf{M}(t) + \mathbf{Q})\mathbf{R}^{-1}(B_0 t)\mathbf{v}_\perp, x_3 - v_3 t)\mu(\mathbf{R}^{-1}(B_0 t)\mathbf{v}_\perp, v_3) d\mathbf{v} d\mathbf{x}, \\ &= \hat{\chi}(\mathbf{k})\hat{\mu}((\mathbf{M}(t) + \mathbf{Q})^\top \mathbf{k}_\perp, k_3 t), \end{aligned}$$

where $\hat{\chi}$ is bounded and the Fourier transform of μ can be explicitly computed:

$$\hat{\mu}((\mathbf{M}(t) + \mathbf{Q})^\top \mathbf{k}_\perp, k_3 t) = \exp\left(-\theta(1 - \cos(B_0 t))(k_1^2 + k_2^2) - \frac{\theta}{2}k_3^2 t^2\right).$$

- For non-Bernstein modes, the above is upper bounded,

$$\hat{\mu}((\mathbf{M}(t) + \mathbf{Q})^\top \mathbf{k}_\perp, k_3 t) \leq e^{-\frac{\theta}{2}k_3^2 t^2},$$

hence

$$\mathcal{E}_\mathbf{k}(t) = \frac{1}{2}|\mathbf{E}_\mathbf{k}|^2 = \frac{1}{2|\mathbf{k}|^2}\hat{\rho}^2(t, \mathbf{k}) \leq \frac{1}{2}|\hat{\chi}(\mathbf{k})|^2|\hat{\mu}((\mathbf{M}(t) + \mathbf{Q})^\top \mathbf{k}_\perp, k_3 t)|^2 \leq C e^{-At^2},$$

for some constant $A, C > 0$.

- For Bernstein modes, i.e. $k_3 = 0$,

$$\hat{\mu}((\mathbf{M}(t) + \mathbf{Q})^\top \mathbf{k}_\perp, k_3 t) = \exp(-\theta(1 - \cos(B_0 t))(k_1^2 + k_2^2)) \leq 1,$$

then the electric energy is periodic and bounded:

$$\mathcal{E}_\mathbf{k}(t) = \frac{1}{2|\mathbf{k}_\perp|^2}|\hat{\chi}(\mathbf{k})|^2 \exp(-2\theta(1 - \cos(B_0 t))(k_1^2 + k_2^2)) \leq \frac{1}{2}|\hat{\chi}(\mathbf{k})|^2.$$

The periodicity is shown in the cos function in the exponential factor, with the period being $\frac{2\pi}{B_0}$.

□

3.2 Control Strategy 2: set c to be constant in (3.6).

To provide an additional concrete realization of the general control design, we propose this section control strategy to set c to be a constant in (3.6). Allowing c to be an arbitrary constant gives a greater flexibility for exercising control.

According to (3.6), this is to set:

$$|\mathbf{k}|^2 L[\hat{\Phi}] + L[\hat{S}] = c\mathbf{k} \cdot (I + L[\hat{\mu}\tilde{\mathbf{R}}])\mathbf{k}. \quad (3.10)$$

We apply inverse Laplace transform, and notice $L^{-1}[1] = \delta(t)$:

$$\hat{\Phi}(t, \mathbf{k}) = -\frac{1}{|\mathbf{k}|^2} \hat{f}_0(\mathbf{k}, (\mathbf{M}(t) + \mathbf{Q})^\top \mathbf{k}_\perp, k_3) + c\delta(t) + c\frac{1}{|\mathbf{k}|^2} \hat{\mu}(\tilde{\mathbf{R}}(t)\mathbf{k})\mathbf{k} \cdot \tilde{\mathbf{R}}(t)\mathbf{k},$$

Using this choice of Φ , we can compute the self-generated field. This is done by plugging it in (3.5) to see:

$$|\mathbf{k}|^2 L[\hat{U}] - L[\hat{S}] = -c\mathbf{k} \cdot L[\hat{\mu}\tilde{\mathbf{R}}\mathbf{k}].$$

Therefore, the self-generated potential has the free-streaming component and a component from propagating the equilibrium state:

$$\hat{U} = \frac{\hat{S}}{|\mathbf{k}|^2} - \frac{1}{|\mathbf{k}|^2} c\mathbf{k} \cdot \hat{\mu}\tilde{\mathbf{R}}\mathbf{k}. \quad (3.11)$$

Remark 3.2 *We should stress that since $\tilde{\mathbf{R}}$ is a 3×3 matrix, the $\mathbf{k} \cdot \tilde{\mathbf{R}}\mathbf{k}$ term cannot easily pull out the $|\mathbf{k}|^2$ component. With more calculation, one can derive:*

$$\mathbf{k} \cdot \tilde{\mathbf{R}}\mathbf{k} = \frac{\sin(B_0 t)}{B_0} |\mathbf{k}_\perp|^2 + k_3^2 t. \quad (3.12)$$

This structure prevents us from directly taking the Fourier inverse transform for an explicit solution for U , as was done in [28] for the Vlasov-Poisson system without external \mathbf{B} .

The performance of this control is not as clean as that of Control Strategy 1. Since it is not able to recover the free-streaming solution, this controlled system maintains nonlinear features, and the performance needs to be discussed case-by-case. Recall the definition of the electric energy of the \mathbf{k} -th mode ($\mathcal{E}_\mathbf{k}(t) = \frac{1}{2} |\mathbf{k}|^2 |\hat{U}_\mathbf{k}|^2$) and the Poisson equation (2.4), following (3.11), we have:

$$\begin{aligned} \mathcal{E}_\mathbf{k}(t) &= \frac{1}{2} |\mathbf{k}|^2 |\hat{U}_\mathbf{k}|^2 = \frac{1}{2} \left| \hat{S} - c\mathbf{k} \cdot \hat{\mu}\tilde{\mathbf{R}}\mathbf{k} \right|^2 \leq |\hat{S}|^2 + c^2 \left| \mathbf{k} \cdot \hat{\mu}\tilde{\mathbf{R}}\mathbf{k} \right|^2 \\ &\leq |\hat{f}_0(\mathbf{k}, (\mathbf{M}(t) + \mathbf{Q})^\top \mathbf{k}_\perp, k_3)|^2 + c^2 |\hat{\mu}|^2 \left| \frac{1}{B_0} |\mathbf{k}_\perp|^2 + k_3^2 t \right|^2. \end{aligned}$$

where we used the definition of S , (2.16) and (3.12). If the initial profile is assumed to be of a factored form as in Theorem 3.1 with μ being a Gaussian, we obtain the following estimate of the temporal behavior of the electric energy:

$$\mathcal{E}_\mathbf{k}(t) \leq \exp\left(-2\theta(1 - \cos(B_0 t))(k_1^2 + k_2^2) - \frac{\theta}{2} k_3^2 t^2\right) \left(|\chi(\mathbf{k})|^2 + c^2 \left| \frac{1}{B_0} |\mathbf{k}_\perp|^2 + k_3^2 t \right|^2 \right).$$

That is, for non-Bernstein modes, $k_3 \neq 0$, the electric energy of the system can be controlled to decay sub-exponentially, at the rate of $O(t^2 e^{-k_3^2 t^2})$. For Bernstein modes, $k_3 = 0$, the electric energy is again controlled to be bounded, $\mathcal{E}_\mathbf{k}(t) \leq |\chi(\mathbf{k})|^2 + \frac{c^2}{B_0^2} |\mathbf{k}_\perp|^4$, but no-decay can be said.

4 Numerical experiments

In this section, we present numerical evidence of the two proposed control strategies.

We choose numerical examples on a $2D2V$ domain by simulating the system for $\mathbf{x} = (x_1, x_2)^\top \in \mathbb{T}^2$, $\mathbf{v} = (v_1, v_2)^\top \in \mathbb{R}^2$:

$$\partial_t F + \mathbf{v} \cdot \nabla_{\mathbf{x}} F + (v_2 B_0 \partial_{v_1} F - v_1 B_0 \partial_{v_2} F) + \mathbf{E} \cdot \nabla_{\mathbf{v}} F(\mathbf{v}) = 0.$$

We test our solution using both Gaussian equilibrium (2.27) and the ring-shaped equilibrium (2.29) for $\mu(\mathbf{v})$. We also set the initial condition to be a small perturbation from such equilibrium states:

$$F(t = 0, \mathbf{x}, \mathbf{v}) = (1 + h(\mathbf{x}))\mu(\mathbf{v}), \quad (4.1)$$

where $h(\mathbf{x})$ denotes the initial perturbation in space, and $|h(\mathbf{x})|$ is taken to be small.

The nonlinear system is computed using a semi-Lagrangian scheme with Strang splitting [32, 33] for the time integration. This means from one step to the next, we first solve

$$\partial_t F + \mathbf{v} \cdot \nabla_{\mathbf{x}} F = 0, \quad (4.2)$$

by $\Delta t/2$, and it is followed by solving

$$\partial_t F + (\mathbf{v} \times \mathbf{B}) \cdot \nabla_{\mathbf{v}} F = 0, \quad (4.3)$$

by $\Delta t/2$ and

$$\begin{cases} \mathbf{E} = -\nabla_{\mathbf{x}} \Delta_{\mathbf{x}}^{-1} (1 - \int F d\mathbf{v}), \\ \partial_t F + \mathbf{E} \cdot \nabla_{\mathbf{v}} F = 0, \end{cases} \quad (4.4)$$

by Δt , before solving (4.3) and (4.2) each by $\Delta t/2$. In \mathbf{x} , we use the Fourier spectrum method, and in \mathbf{v} , we perform linear interpolation.

The code is written in JAX, and the computation was performed on an NVIDIA Quadro RTX 6000 GPU with 24 GB of memory. The data and code for results presented here are openly available in the GitHub repository², and archived in Zenodo³.

4.1 Dory-Guest-Harris instability.

This section is dedicated to the cases where μ is chosen as a ring-shaped equilibrium (2.29) with index $j = 6$ (hence termed DGH6). The two subsections 4.1.1 and 4.1.2 use different initial perturbations, and we apply two different control strategies to showcase the prediction of our theory.

²https://github.com/Peiyi-wisc/Magnetized_VP_control.git

³<https://doi.org/10.5281/zenodo.15109942>

4.1.1 Initial perturbation as a sine wave in space

In this example we set $B_0 = 0.05$, and use the following initial condition:

$$F_0(\mathbf{x}, \mathbf{v}) = (1 + 0.001 \sin(0.1x_1)) \frac{1}{\pi 6! / 3} \left(\frac{v_1^2 + v_2^2}{1/3} \right)^6 \exp\left(-\frac{v_1^2 + v_2^2}{1/3} \right). \quad (4.5)$$

For simulation we use $x_1, x_2 \in [-10\pi, 10\pi]$, $v_1, v_2 \in [-5, 5]$, $N_{x_1} = N_{x_2} = 64$, $N_{v_1} = N_{v_2} = 64$.

Without control, we observe that the electric energy exponentially grows in time, as shown in Figure 3. In Figure 4, we present a slice of distribution $f(x_1, v_1)$ by setting $(x_2, v_2) = (0, 0)$. The distribution starts showing turbulent features as early as $t = 300$, and deforms as time evolves. In Figure 5, we plot a 3D plot by fixing $x_2 = 0$, and it is clear that the ring-shape distribution is deformed at $T = 400$.

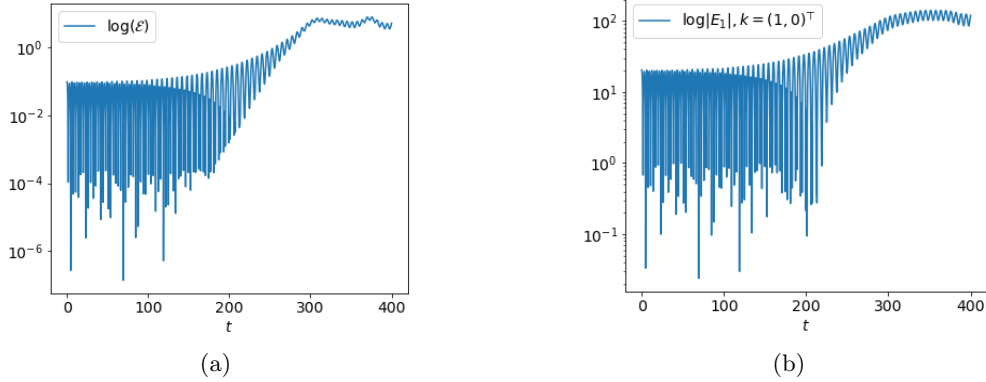


Fig. 3: The left panel shows the evolution of the electric energy $\mathcal{E}(t)$, and the right panel shows the first coordinate of $|\mathbf{E}_{(1,0)^T}(t)|$. Both plots are presented on the semi-log scale.

We apply Control Strategy 1 by setting $c = 0$ first. This eliminates all the poles, and as suggested by Theorem 3.1, it should recover the free-streaming solution, whose energy is expected to be bounded and periodic (Bernstein modes). In Figures 6, 7 and 8, we respectively show the counterparts for the case without the control. More specifically, it is clear in Figure 6 that energy is no longer growing. While the slice distribution of $f(x_1, x_2 = 0, v_1, v_2 = 0)$ continues showing the two-beam structure, the full ring is deformed, as seen in Figure 7 and Figure 8.

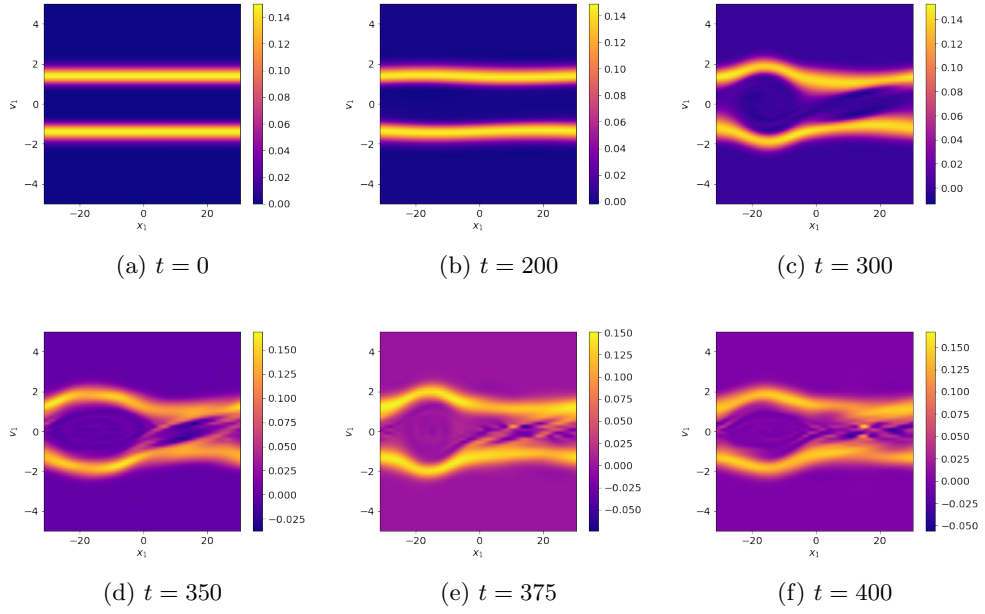


Fig. 4: Distribution $f(x_1, x_2 = 0, v_1, v_2 = 0)$ snapshot at different time steps, without control. The distribution is asymmetric in the spatial domain, and the effect is rooted in the asymmetry in the perturbation in the initial data.

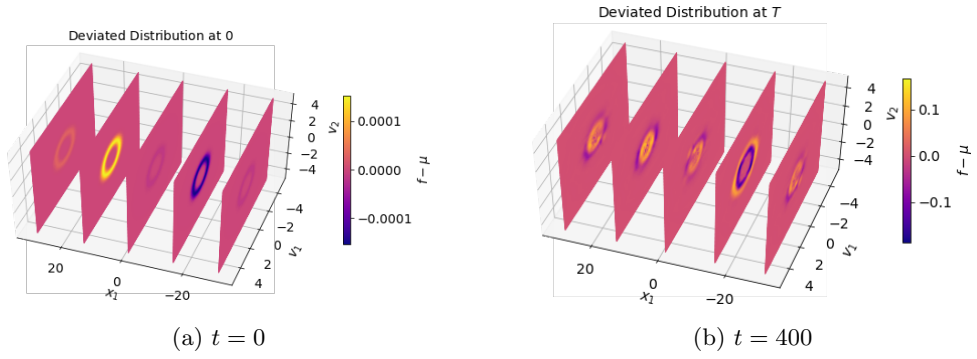


Fig. 5: Distribution $f(x_1, x_2 = 0, v_1, v_2)$ at five x_1 locations, without control.

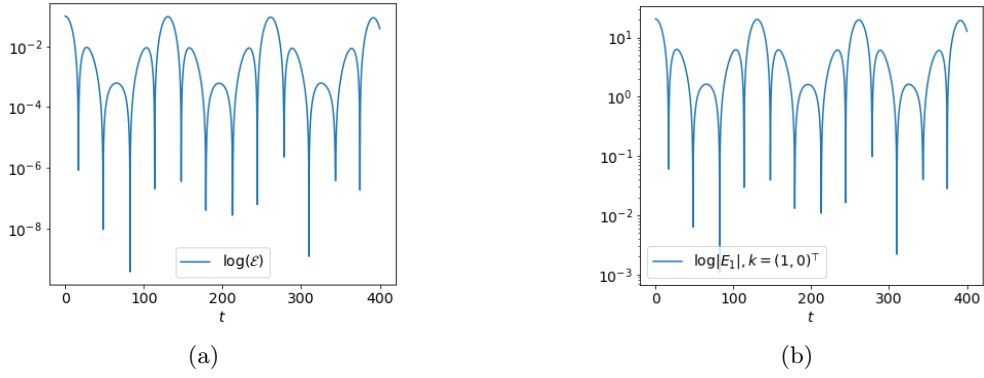


Fig. 6: Evolution of the electric energy $\mathcal{E}(t)$, and the first coordinate of $|\mathbf{E}_{(1,0)^\top}(t)|$ in semi-log scale, with Control Strategy 1 that $c = 0$.

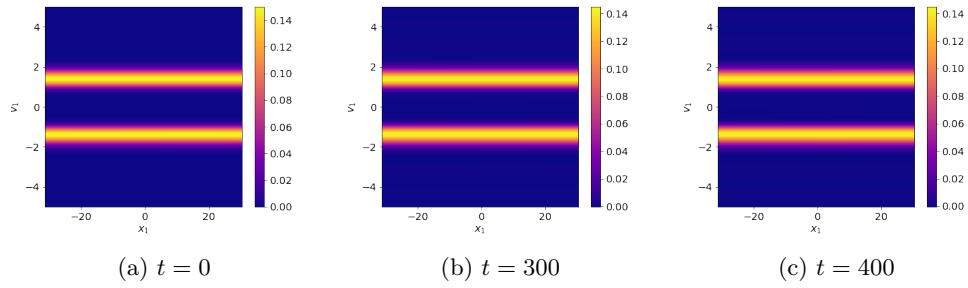


Fig. 7: Distribution $f(x_1, x_2 = 0, v_1, v_2 = 0)$ snapshot at different time steps, with Control Strategy 1 that $c = 0$.

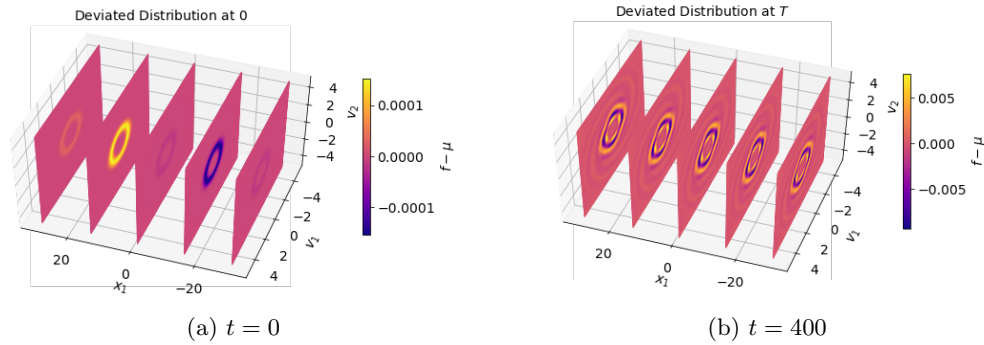


Fig. 8: Distribution $f(x_1, x_2 = 0, v_1, v_2)$ at five x_1 locations, with control $c = 0$.

4.1.2 Initial perturbation as a Gaussian in space.

We then examine an example with the ring-shaped equilibrium and perturbed initially by a Gaussian in space \mathbf{x} :

$$F_0(\mathbf{x}, \mathbf{v}) = \left(1 + 0.01 \frac{1}{2\pi\theta_0} e^{-\frac{\mathbf{x}^2}{2\theta_0}}\right) \frac{1}{\pi 6!/3} \left(\frac{v_1^2 + v_2^2}{1/3}\right)^6 \exp\left(-\frac{v_1^2 + v_2^2}{1/3}\right).$$

We set $B_0 = 0.05$. From analysis in Section 2.2.2, this equilibrium is not stable, and we expect the dynamics to present the Dory-Guest-Harris instability, and that the electric energy $\mathcal{E}(t)$ and $|\mathbf{E}_1(\mathbf{k})|$ for $\mathbf{k} = (1, 0)^\top$ are expected to grow exponentially in time. This is shown in Figure 9. We also plot the evolution of density ρ in Figure 10. The initial perturbation is a Gaussian at the origin, and the magnitude variation in ρ highly concentrates at $\mathbf{x} = 0$. Once we kick off the dynamics, the Gaussian beam starts propagating outward and forms a ring-shaped distribution. The magnitude of variation in ρ very soon ($t = 10$) drops down to 10^{-5} . In time, turbulence begins to take effect, and the variation is about 10^{-4} at about $t = 300$ and 400 .

We now present the simulation with control. Recalling 3.2, the external control electric potential is

$$\hat{\Phi}(t, \mathbf{k}) = -\hat{S} + c\delta(t) + c \frac{\sin(B_0 t)}{B_0} \hat{\mu}(\tilde{\mathbf{R}}(t)\mathbf{k}).$$

Setting $c = 0$ in (3.6) returns the Control Strategy 1. We will examine different effects when c is set at different values.

When $c = 0$, the corresponding electric energy and Fourier mode coefficient are presented in Figure 12(a)(e). The electric energy is suppressed under 10^{-5} for all time, and the density profile has much less variation comparing Figure 11 to Figure 10.

We also tested setting c to be at different values. The results are shown in Figure 12, with $c = 0.001, c = 0.005, c = 0.01$. For all these tests, the electric energy can be controlled below the level of 10^{-5} for all time, thus suppressing the instability as in Figure 9. However, we also notice that in Figure 12(d)(h), for c being 0.01, the electric energy gradually grows after $t = 300$. This indicates that the perturbation induced by the term $c \frac{\sin(B_0 t)}{B_0} \hat{\mu}$ in (3.10) might lead to another instability in the system.

4.2 Gaussian equilibrium

Gaussian equilibrium is expected to be a linearly stable equilibrium state according to the linear analysis when the initial perturbation is small. We now study the situation when a large perturbation is posed on the Gaussian equilibrium. This is beyond the linear stable regime, and potential instability may be observed. This is indeed the case. We set $B_0 = 1$, adopt the Kelvin-Helmholtz type instability example in [34] and use the following initial condition:

$$F(t = 0, \mathbf{x}, \mathbf{v}) = (1 + 0.0015 \cos(0.4x_1) + 0.15 \sin(x_2)) \frac{1}{2\pi} e^{-\frac{v_1^2 + v_2^2}{2}},$$

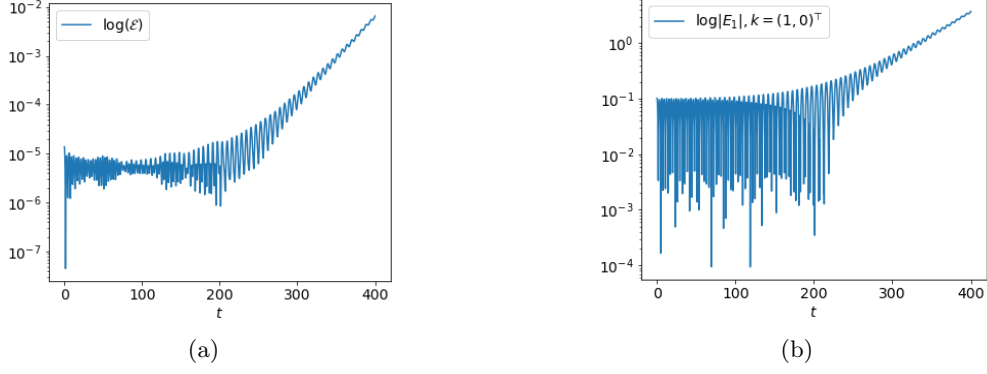


Fig. 9: Evolution of the electric energy $\mathcal{E}(t)$, and the first coordinate of $|\mathbf{E}_{(1,0)^\top}(t)|$ in semi-log scale, without control.

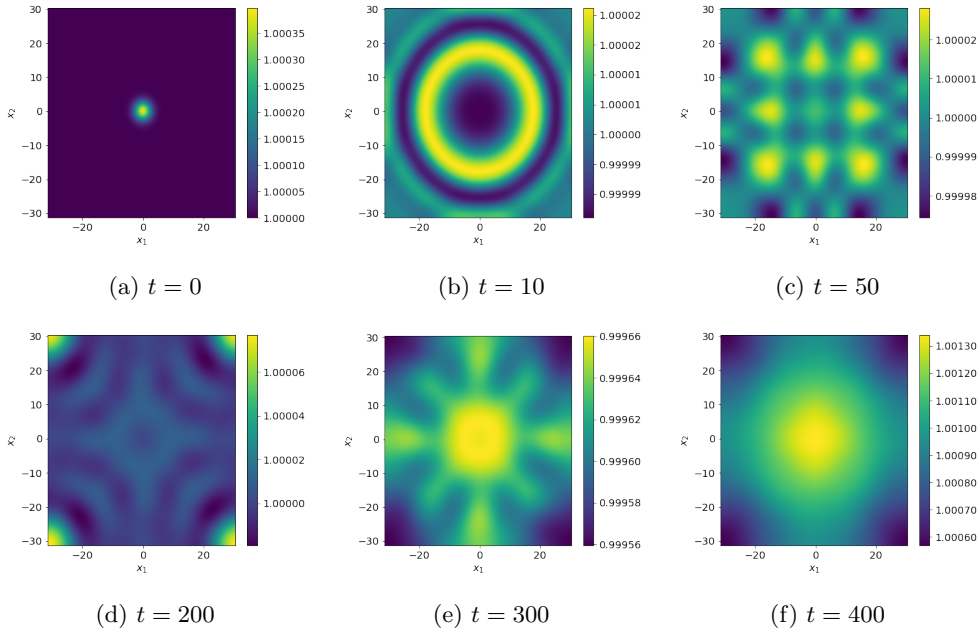


Fig. 10: Density $\rho(x_1, x_2)$ snapshot at different time steps, without control.

where $x_1 \in [-2.5\pi, 2.5\pi]$, $x_2 \in [-\pi, \pi]$, $v_1, v_2 \in [-5, 5]$. For numerical discretization, we use $N_{x_1} = 64$, $N_{x_2} = 16$, $N_{v_1} = N_{v_2} = 64$ and run the simulation till terminal time $T = 400$. Without any control, we present the electric energy, together with the Fourier coefficient $|\mathbf{E}_{(1,0)^\top}|$ in Figure 13. The specific feature of Bernstein modes is still evident, in the sense that the electric energy is bounded and oscillatory, i.e., no damping. However, exponential growth is observed for certain Fourier modes, such as

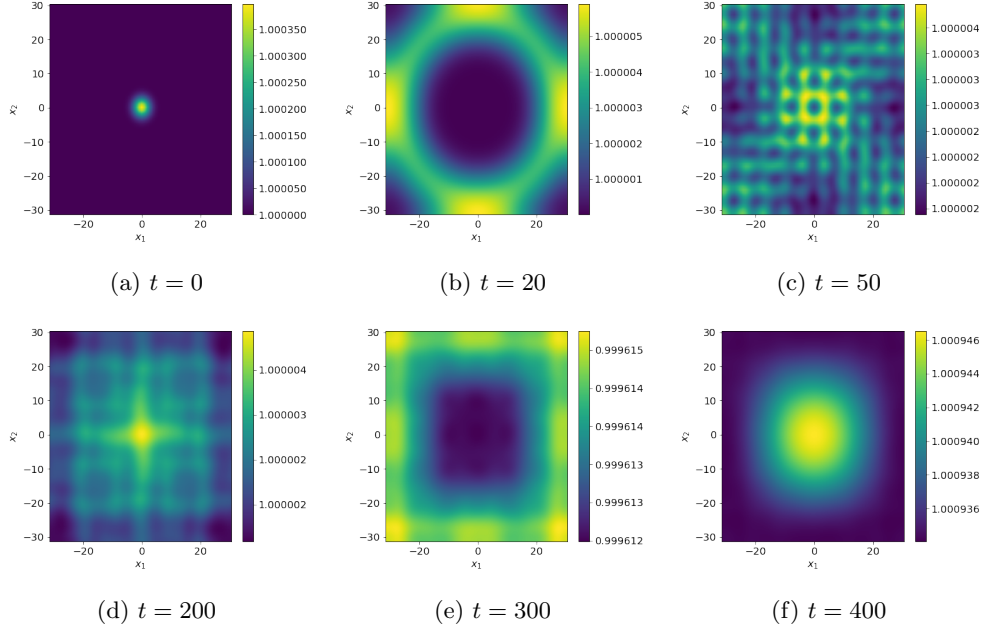


Fig. 11: Density $\rho(x_1, x_2)$ snapshot at different time steps, with Control Strategy 1 that $c = 0$.

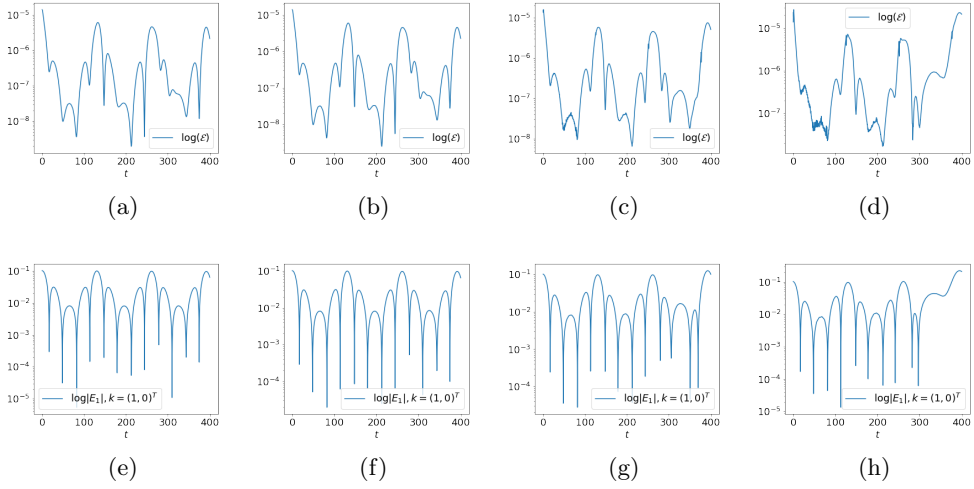


Fig. 12: Evolution of the electric energy $\mathcal{E}(t)$, and the first coordinate of $|\mathbf{E}_{(1,0)^\top}(t)|$ in semi-log scale, control with different c values. Panel (a)(e): $c = 0$, Panel (b)(f): $c = 0.001$, Panel (c)(g): $c = 0.005$, Panel (d)(h): $c = 0.01$.

$\mathbf{k} = (1, 0)^\top$ in Panel (b). We also plot six time slots of the density ρ in Figure 14. According to the initial distribution formula, the initial density is in the shape of a sine wave in the x_2 direction, but the perturbation in the x_1 direction is negligible. However, as the dynamics continues, perturbations in the x_1 direction become more and more noticeable. A full 3D distribution (set $x_2 = 0$) at initial time $t = 0$ and final time $t = 400$ is shown in Figure 15 (a)(b).

We then apply Control Strategy 1 to the above system. According to Remark 3.1, the control is expected to be effective, as will be shown below in numerical results. In Figure 16, it is clear that the electric energy and $\mathbf{k} = (1, 0)^\top$ continue being oscillatory, but the magnitude decays in time, and thus is suppressed. The density profile is also much smoother, as seen in Figure 17. It is kept close to the initial perturbation for all time, and there is no mixing compared to Figure 14. According to Figure 15 (a)(c), where we present the initial and final 3D distribution (with fixed $x_2 = 0$), it is also clear that turbulence no longer exists.

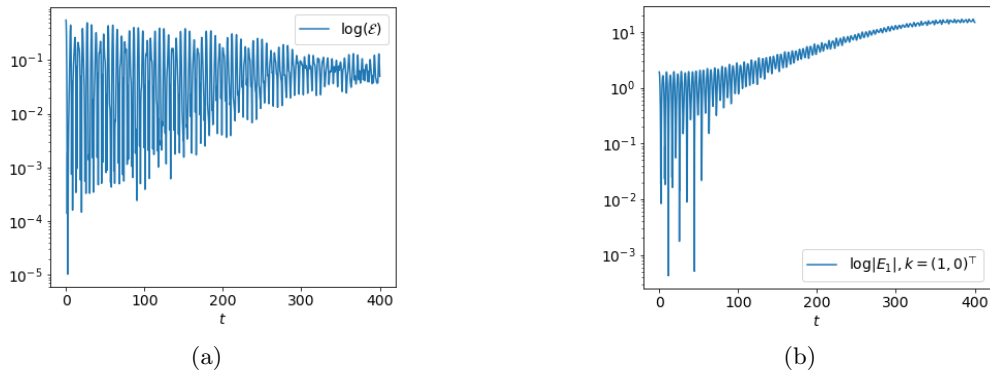


Fig. 13: Evolution of the electric energy $\mathcal{E}(t)$, and the first coordinate of $|\mathbf{E}_{(1,0)^\top}(t)|$ in semi-log scale, without control.

5 Conclusion

This paper studies the stabilization and control of plasma dynamics in the presence of an external magnetic field, modeled by the magnetized Vlasov–Poisson system. We derived the corresponding dispersion relation and formulated the associated Penrose-type stability condition (Proposition 2.2). As representative examples, we considered two equilibrium distributions: a Gaussian equilibrium and a ring-shaped equilibrium. The latter admits an unstable root in the dispersion relation, leading to linear instability (the Dory–Guest–Harris instability) and exponential growth of the electric energy in the linear regime.

Building on this analysis, we investigated the control problem of suppressing instability through an externally imposed electric field. The dispersion relation provides a central tool for the design of such controls. We proposed two control strategies, both

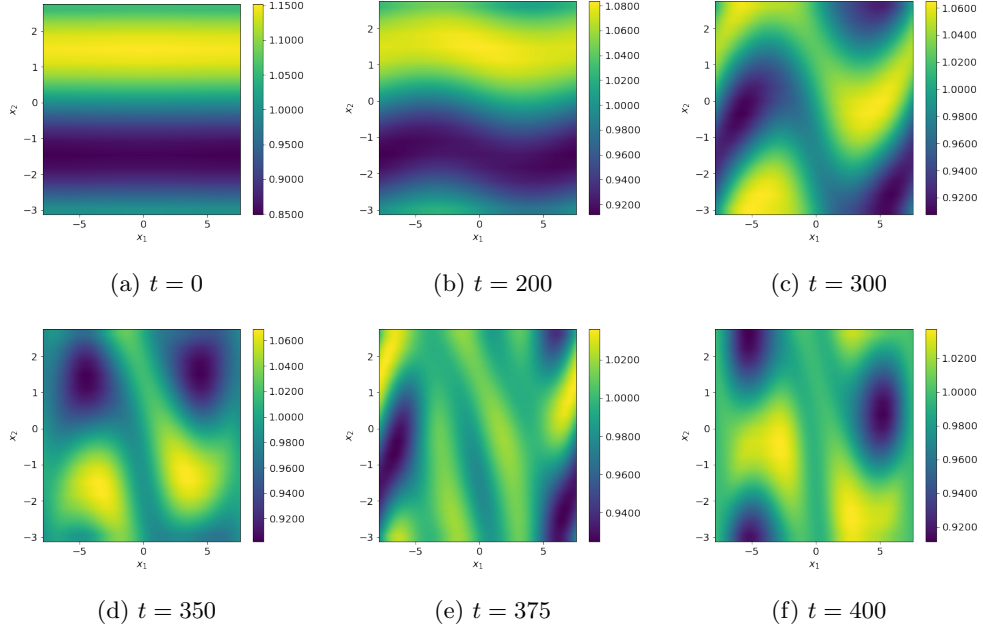


Fig. 14: Density $\rho(x_1, x_2)$ snapshot at different time steps, without control.

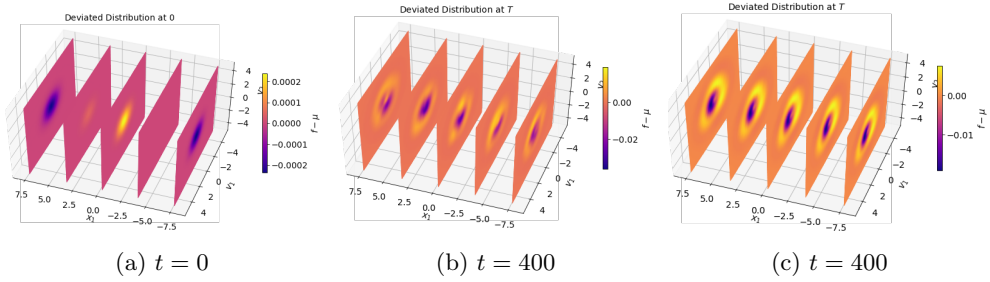


Fig. 15: The deviated distribution function $f(x_1, x_2 = 0, v_1, v_2) - \mu$ at five x_1 locations. Panels (a) and (b) show the deviated distribution without control at time $t = 0$ and $t = 400$, respectively. Panels (a) and (c) show the deviated distribution with Control Strategy 1, that $c = 0$.

based on eliminating unstable roots in the dispersion relation. One of these strategies recovers the free-streaming solution as a special case, which further enables an explicit characterization of the electric energy and a proof that it remains bounded. Numerical experiments demonstrate the effectiveness of the proposed strategies and indicate that stabilization persists beyond the strictly linear regime, including in certain nonlinear settings.

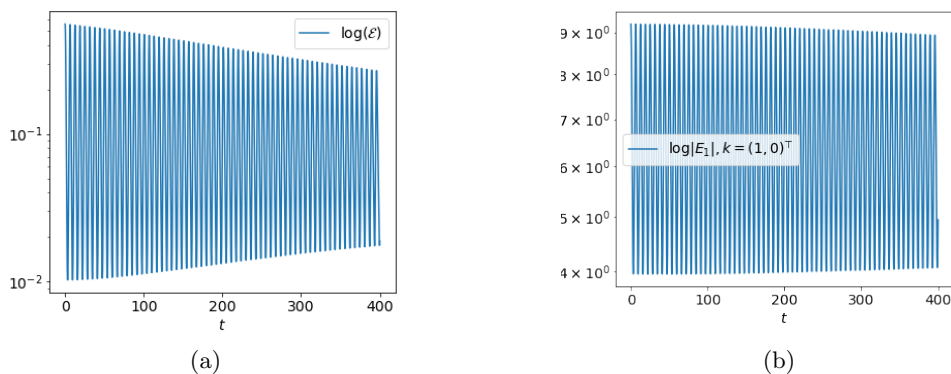


Fig. 16: Evolution of the electric energy $\mathcal{E}(t)$, and the first coordinate of $|\mathbf{E}_{(1,0)^\top}(t)|$ in semi-log scale, with Control Strategy 1 that $c = 0$.

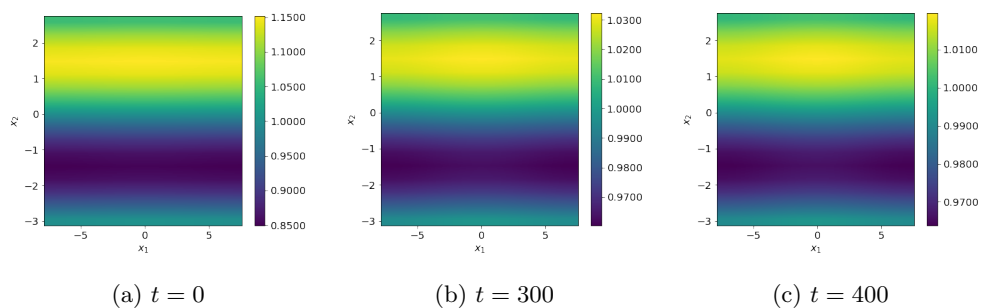


Fig. 17: Density $\rho(x_1, x_2)$ snapshot at different time steps, with Control Strategy 1 that $c = 0$.

Stabilizing plasma dynamics via external fields is a key component in the broader objective of controlled fusion. While the present work is carried out in an idealized setting, it provides a step toward systematic control design in higher-dimensional kinetic models relevant to fusion applications. An important future direction is to extend the pole-elimination methodology to reduced descriptions such as drift-kinetic and gyrokinetic regimes, where the presence of multiple time and length scales introduces additional analytical and computational challenges. On the computational side, advancing to gyrokinetic scaling will likely require efficient large-scale solvers, potentially accelerated by GPU-based implementations.

Acknowledgements

P.C. thanks Genia Vogman, Xiaochuan Tian, and Qihao Ye for useful discussions on the Dory-Guest-Harris instability and related details. R.J. is supported by the National

Science Foundation under Grant No. 2409066. P.C., Q.L., and Y.Y. are supported by the National Science Foundation under Grant No.2308440.

Declarations

The authors have no competing interests to declare that are relevant to the content of this article.

Appendix A Computation of $P(\mathbf{k}, \lambda)$

A.1 Fourier transform of ring-shaped μ (2.28)

In this subsection, we present the details to compute the Fourier transform of the ring-shaped distribution (2.28).

Note that μ is radial symmetric in \mathbf{v} , we change to polar coordinates, then

$$\begin{aligned}\hat{\mu}(\mathbf{k}) &= \frac{1}{\pi\alpha_{\perp}^2 j!} \int_{\mathbb{R}^2} e^{-i(k_1 v_1 + k_2 v_2)} \left(\frac{v_1^2 + v_2^2}{\alpha_{\perp}^2} \right)^j \exp\left(-\frac{v_1^2 + v_2^2}{\alpha_{\perp}^2}\right) d\mathbf{v}, \\ &= \frac{1}{\pi\alpha_{\perp}^2 j!} \frac{1}{\alpha_{\perp}^{2j}} \int_0^{\infty} \int_0^{2\pi} e^{-i(k_1 v_r \cos \theta + k_2 v_r \sin \theta)} v_r^{2j} \exp\left(-\frac{v_r^2}{\alpha_{\perp}^2}\right) v_r dv_r d\theta, \\ &= \frac{1}{\pi j!} \int_0^{\infty} \int_0^{2\pi} e^{-i\alpha_{\perp} w_r |\mathbf{k}| \sin(\theta)} d\theta w_r^{2j+1} \exp(-w_r^2) dw_r, \quad (w_r := \frac{v_r}{\alpha_{\perp}}) \\ &= \frac{2}{j!} \int_0^{\infty} J_0(\alpha_{\perp} |\mathbf{k}| w_r) w_r^{2j+1} \exp(-w_r^2) dw_r,\end{aligned}$$

where $J_0(\cdot)$ is the zeroth-order Bessel function of the first kind, and we use the integral representation of Bessel functions. Thus in (2.6),

$$\begin{aligned}\hat{\mu}(\tilde{\mathbf{R}}\mathbf{k}) &= \frac{2}{j!} \int_0^{\infty} J_0(\alpha_{\perp} |\tilde{\mathbf{R}}\mathbf{k}| w_r) w_r^{2j+1} \exp(-w_r^2) dw_r, \\ &= M(j+1, 1, -\frac{\alpha_{\perp}^2 |\tilde{\mathbf{R}}\mathbf{k}|^2}{4}) = \exp\left(-\frac{\alpha_{\perp}^2 |\tilde{\mathbf{R}}\mathbf{k}|^2}{4}\right) M(-j, 1, \frac{\alpha_{\perp}^2 |\tilde{\mathbf{R}}\mathbf{k}|^2}{4}),\end{aligned}$$

here $M(\cdot, \cdot, \cdot)$ is the Kummer's function (or the hypergeometric function), the last line is obtained in [35] together with Kummer's transform. One specific property of Kummer's function is that for j being nonnegative integers, $M(-j, \cdot, \cdot)$ can be expressed as a polynomial of degree no more than j .

In the case of $j = 6$ (2.29), the analytical expression of M is a polynomial of power 6:

$$M(-6, 1, z) = \sum_{n=0}^6 \frac{(-1)^n 6! / n!}{(n!)^2} z^n = 1 - 6z + \frac{15}{2}z^2 - \frac{10}{3}z^3 + \frac{5}{8}z^4 - \frac{1}{20}z^5 + \frac{1}{6!}z^6,$$

where $z = \frac{\alpha_{\perp}^2 |\tilde{\mathbf{R}}\mathbf{k}|^2}{4} = \frac{1}{6B_0^2} |\mathbf{k}|^2 (1 - \cos(B_0 t))$.

References

- [1] Solov'ev, V.D. L. S. and Shafranov: In: Leontovich, M.A. (ed.) *Plasma Confinement in Closed Magnetic Systems*, pp. 1–247. Springer, Boston, MA (1995)
- [2] Zohm, H.: *Magnetohydrodynamic Stability of Tokamaks*. Wiley-VCH, Weinheim (2015). <https://doi.org/10.1002/9783527677375>
- [3] Freidberg, J.P.: *Plasma Physics and Fusion Energy*. Cambridge University Press, Cambridge (2007)
- [4] Wesson, J.: *Tokamaks*. Oxford University Press, New York (2004)
- [5] Rogers, B.N., Ricci, P.: Low-frequency turbulence in a linear magnetized plasma. *Phys. Rev. Lett.* **104**, 225002 (2010) <https://doi.org/10.1103/PhysRevLett.104.225002>
- [6] Schaeffer, J.: Global existence of smooth solutions to the Vlasov–Poisson system in three dimensions. *Comm. Partial Differential Equations* **16**(8-9), 1313–1335 (1991) <https://doi.org/10.1080/03605309108820801>
<https://doi.org/10.1080/03605309108820801>
- [7] Pfaffelmoser, K.: Global classical solutions of the vlasov-poisson system in three dimensions for general initial data. *J. Differential Equations* **95**(2), 281–303 (1992) [https://doi.org/10.1016/0022-0396\(92\)90033-J](https://doi.org/10.1016/0022-0396(92)90033-J)
- [8] Mouhot, C., Villani, C.: On Landau damping. *Acta Math.* **207**(1), 29–201 (2011)
- [9] Skubachevskii, A.L.: Nonlocal problems for the Vlasov–Poisson equations in an infinite cylinder. *Funct. Anal. Appl.* **49**(3), 234–238 (2015)
- [10] Belyaeva, Y.O., Skubachevskii, A.L.: Unique solvability of the first mixed problem for the Vlasov–Poisson system in infinite cylinder. *J. Math. Sci.* **244**(6), 930–945 (2020)
- [11] Belyaeva, Y.O., Gebhard, B., Skubachevskii, A.L.: A general way to confined stationary Vlasov–Poisson plasma configurations. *Kinet. Relat. Models* **14**(2), 257–282 (2021) <https://doi.org/10.3934/krm.2021004>
- [12] Bedrossian, J., Wang, F.: The linearized Vlasov and Vlasov–Fokker–Planck equations in a uniform magnetic field. *J. Stat. Phys.* **178**(2), 552–594 (2020)
- [13] Dory, R.A., Guest, G.E., Harris, E.G.: Unstable electrostatic plasma waves propagating perpendicular to a magnetic field. *Phys. Rev. Lett.* **14**, 131–133 (1965) <https://doi.org/10.1103/PhysRevLett.14.131>

- [14] Tataronis, J.A., Crawford, F.W.: Cyclotron harmonic wave propagation and instabilities: I. perpendicular propagation. *J. Plasma Phys.* **4**(2), 231–248 (1970) <https://doi.org/10.1017/S0022377800004979>
- [15] Vogman, G.V., Colella, P., Shumlak, U.: Dory–Guest–Harris instability as a benchmark for continuum kinetic Vlasov–Poisson simulations of magnetized plasmas. *J. Comput. Phys.* **277**, 101–120 (2014) <https://doi.org/10.1016/j.jcp.2014.08.014>
- [16] Bernstein, I.B.: Waves in a plasma in a magnetic field. *Phys. Rev.* **109**, 10–21 (1958) <https://doi.org/10.1103/PhysRev.109.10>
- [17] Sukhorukov, A.I., Stubbe, P.: On the Bernstein–Landau paradox. *Phys. Plasmas* **4**(7), 2497–2507 (1997) <https://doi.org/10.1063/1.872229>
- [18] Horton, W., Perez, J.C., Carter, T., Bengtson, R.: Vorticity probes and the characterization of vortices in the Kelvin–Helmholtz instability in the large plasma device experiment. *Phys. Plasmas* **12**(2), 022303 (2005) <https://doi.org/10.1063/1.1830489>
- [19] Perez, J.C., Horton, W., Bengtson, R.D., Carter, T.: Study of strong cross-field sheared flow with the vorticity probe in the Large Plasma Device. *Phys. Plasmas* **13**(5), 055701 (2006) <https://doi.org/10.1063/1.2179423>
- [20] Brochard, F., Gravier, E., Bonhomme, G.: Transition from flute modes to drift waves in a magnetized plasma column. *Phys. Plasmas* **12**(6), 062104 (2005) <https://doi.org/10.1063/1.1921167>
- [21] Pueschel, M.J., Rossi, G., Told, D., Terry, P.W., Jenko, F., Carter, T.A.: A basic plasma test for gyrokinetics: GDC turbulence in LAPD. *Plasma Phys. Control. Fusion* **59**(2), 024006 (2017) <https://doi.org/10.1088/1361-6587/aa52e6>
- [22] Bedrossian, J., Masmoudi, N., Mouhot, C.: Landau damping: paraproducts and Gevrey regularity. *Ann. PDE* **2**(1), 4 (2016) <https://doi.org/10.1007/s40818-016-0008-2>
- [23] Einkemmer, L., Li, Q., Wang, L., Yang, Y.: Suppressing instability in a Vlasov–Poisson system by an external electric field through constrained optimization. *J. Comput. Phys.* **498**, 112662 (2024) <https://doi.org/10.1016/j.jcp.2023.112662>
- [24] Knopf, P.: Optimal control of a Vlasov–Poisson plasma by an external magnetic field. *Calc. Var. Partial Differential Equations* **57**(5), 134 (2018)
- [25] Knopf, P., Weber, J.: Optimal control of a Vlasov–Poisson plasma by fixed magnetic field coils. *Appl. Math. Optim.* **81**(3), 961–988 (2020)

- [26] Bartsch, J., Knopf, P., Scheurer, S., Weber, J.: Controlling a Vlasov–Poisson plasma by a Particle-in-Cell method based on a Monte Carlo framework. *SIAM J. Control Optim.* **62**(4), 1977–2011 (2024) <https://doi.org/10.1137/23M1563852>
- [27] Albi, G., Dimarco, G., Ferrarese, F., Pareschi, L.: Instantaneous control strategies for magnetically confined fusion plasma. *J. Comput. Phys.* **527**, 113804 (2025) <https://doi.org/10.1016/j.jcp.2025.113804>
- [28] Einkemmer, L., Li, Q., Mouhot, C., Yue, Y.: Control of instability in a Vlasov–Poisson system through an external electric field. *J. Comput. Phys.* **530**, 113904 (2025) <https://doi.org/10.1016/j.jcp.2025.113904>
- [29] Davies, B.: *Integral Transforms and Their Applications*. Texts in Applied Mathematics. Springer, New York (2002)
- [30] Crawford, F.W., Tataronis, J.A.: Absolute instabilities of perpendicularly propagating cyclotron harmonic plasma waves. *J. Appl. Phys.* **36**(9), 2930–2934 (1965) <https://doi.org/10.1063/1.1714609>
- [31] Tataronis, J.A., Crawford, F.W.: Cyclotron harmonic wave propagation and instabilities: I. perpendicular propagation. *J. Plasma Phys.* **4**(2), 231–248 (1970) <https://doi.org/10.1017/S0022377800004979>
- [32] Crouseilles, N., Mehrenberger, M., Sonnendrücker, E.: Conservative semi-Lagrangian schemes for Vlasov equations. *J. Comput. Phys.* **229**(6), 1927–1953 (2010) <https://doi.org/10.1016/j.jcp.2009.11.007>
- [33] Einkemmer, L.: A performance comparison of semi-Lagrangian discontinuous Galerkin and spline based Vlasov solvers in four dimensions. *J. Comput. Phys.* **376**, 937–951 (2019) <https://doi.org/10.1016/j.jcp.2018.10.012>
- [34] Vu, A.-T., Mehrenberger, M.: Semi-Lagrangian Vlasov–Poisson solvers with a strong external uniform magnetic field. preprint (2023). <https://hal.science/hal-04016348>
- [35] Gradshteyn, I.S., Ryzhik, I.M.: Chapter 6 - Definite integrals of special functions. In: Zwillinger, D., Moll, V. (eds.) *Table of Integrals, Series, and Products*, 8th edn., pp. 637–775. Academic Press, Boston (2014). <https://doi.org/10.1016/B978-0-12-384933-5.00006-0>